

# DOUBLE ELECTRIC LAYER IN THE STATIONARY SHOCK WAVE STRUCTURES OF A SUPERSONIC FLOW

D. Janette Drake

ADVISOR: L. Vušković

Department of Physics  
Old Dominion University  
4600 Elkhorn Ave, Norfolk, VA 23529

Understanding the interaction between a weakly ionized gas and a shock wave is important for detailed knowledge of the conditions of planetary atmospheric entry. This interaction can manifest itself in the form of a localized increase of electron temperature, plasma induced shock dispersion and acceleration, optical emission enhancement, or double electric layers. In our work, a microwave discharge was combined with the flow tube to sustain a supersonic flow of ionized gas. Stationary shocks formed in front of a spherical model. Argon and Ar/H<sub>2</sub> (95/5%) mixture were used as test gases. Excited state populations of the argon (4p-4s) spectral lines were measured across the stationary shock by employing absolute emission spectroscopy. We compared measured intensity in the subsonic and the supersonic regions of the flow and observed dispersion effects in the form of a double-peak distribution. Kinetic modeling of the discharge was performed and the associated transport parameters and rate coefficients were calculated.

It is known that shock waves in a weakly ionized gas generate double electric layers due to the separation and redistribution of space charge across the shock layer. Additionally, plasma induced shock dispersion and optical emission enhancement can also be produced by the interaction of an acoustic shock wave and a weakly ionized gas. These effects could be present at any planetary atmospheric entry. So far the double electric layer has not been studied in detail in the context of planetary entry plasma

Many experiments have been performed with the aim to understand the interaction of a shock wave and a weakly ionized gas, in view of the possible applications to high speed aerodynamics. A number of these experiments have noted the effects of temperature on the shock wave as well as

localized increase of electron temperature at the shock fronts.<sup>1-3</sup> Our experiments with supersonic flowing afterglow,<sup>4-7</sup> and the experiments by Bletzinger *et al.*<sup>8,9</sup> indicate an excessive increase of radiation from the electronically excited states across the shock layer. This increase could not be explained by the linear approximation, where the height of potential barrier in the double layer was of the order of the electron temperature in the unperturbed plasma. Siefert *et al.*<sup>10</sup> proposed a hypothesis of a strong double electric layer, based on the interactions between heavy particles in the plasma-shock region.

The primary objective of our investigation is to validate the hypothesis of the strong double electric layer. We are investigating a stationary shock wave formed by a blunt model in a supersonic flow, as opposed to the

traveling shock wave arrangement described in Ref. [11]. Our aim is to determine the location of the shock front in the plasma in relation to the model. We expect that we will observe the dispersion of the stationary shock wave in front of the model. Additionally, we expect to see an enhancement of optical emission at the shock front, which is an indicator of a double electric layer.

### Kinetic Modeling

In developing the model we start from the Boltzmann Transport Equation,

$$\begin{aligned} & \frac{\partial f(\vec{r}, \vec{v}, t)}{\partial t} + \vec{v} \cdot \vec{\nabla} f(\vec{r}, \vec{v}, t) - \frac{e\vec{E}}{m} \cdot \vec{\nabla} f(\vec{r}, \vec{v}, t) \\ & = \left( \frac{\partial f(\vec{r}, \vec{v}, t)}{\partial t} \right)_{coll} \end{aligned} \quad (1)$$

Here the distribution of electrons in their velocity space  $\vec{v}$  at the space coordinate  $\vec{r}$  and at time  $t$  is given by the electron velocity distribution function  $f(\vec{r}, \vec{v}, t)$ . In the case of a weakly ionized gas, the right hand side of Eq. (1) will take into account the elastic and inelastic collisions between electrons and neutral atoms or molecules.

Due to the complexity of Eq. (1), solutions can only be determined for selected cases. Approximations, such as the homogenous approximation, are usually employed. In our case, a steady state approximation is valid when the electron collision frequency in the discharge is approximately two or three orders of magnitude larger than the driving frequency. Additionally, we can make the assumption of symmetry about the discharge axis. By applying these approximations, a steady state isotropic solution can be obtained for a monatomic gas,<sup>12</sup>

$$\begin{aligned} & \frac{1}{3} \left( \frac{eE}{N} \right)^2 \frac{d}{d\varepsilon} \left( \frac{\varepsilon}{Q_m} \frac{df}{d\varepsilon} \right) + \frac{2mkT}{M} \frac{d}{d\varepsilon} \left( \varepsilon^2 Q_m \frac{df}{d\varepsilon} \right) \\ & + \frac{2m}{M} \frac{d}{d\varepsilon} (\varepsilon^2 Q_m f) - \varepsilon f(\varepsilon) \sum_j Q_j(\varepsilon) \\ & + \sum_j (\varepsilon + \varepsilon_j) f(\varepsilon + \varepsilon_j) Q_j(\varepsilon + \varepsilon_j) = 0. \end{aligned} \quad (2)$$

Here we have expressed, by convention, the solution in terms of the electron energy  $\varepsilon = mv^2/2$  and have neglected super-elastic collisions. In Eq. (2),  $Q_m$  is the momentum transfer cross section;  $Q_j$  is the cross section of the  $j^{\text{th}}$  inelastic collision;  $m$ ,  $e$  are the mass and charge of the electron;  $M$ ,  $N$ , and  $T$  are the mass, density, and temperature of the neutral gas molecules;  $k$  is the Boltzmann constant; and  $f$  is the isotropic electron energy distribution function (EEDF).

For a gas mixture, an appropriate modification to the cross sections of all gas species in Eq. (2) should be made:  $Q_m = \sum_n Q_m^n G^n$  in the first term and  $Q_m = \sum_n M Q_m^n G^n / M^n$  and  $M = \sum_n M^n G^n$  in the second and third terms.

Here  $Q_m^n$  is the momentum transfer cross section,  $G^n$  is the mole fraction, and  $M^n$  is the mass of the molecule of the  $n^{\text{th}}$  species.<sup>13</sup>

We will calculate the EEDF by employing a commercial numerical Boltzmann solver, Bolsig,<sup>1</sup> for weakly ionized gases. Bolsig provides numerical solutions for the EEDF at different values of the reduced electric field ( $E/N$ ). From these values we are able to estimate the average electron temperature ( $T_e$ ) of the distribution and rate constants ( $k_j$ ) for certain processes,

<sup>1</sup> <http://www.siglo-kinema.com/bolsig.htm>

$$T_e = \frac{2}{3} \int_0^{\infty} \varepsilon^{3/2} f(\varepsilon) d\varepsilon \quad (3)$$

$$k_j = \left( \frac{2e}{m} \right)^{1/2} \int_0^{\infty} \varepsilon Q_j(\varepsilon) f(\varepsilon) d\varepsilon. \quad (4)$$

To verify the accuracy of the numerical results, we present in Fig. 1 a comparison of the results from Bolsig with calculated results from a Ref. [14]. We found that the Bolsig data lined up very well with these calculated values.

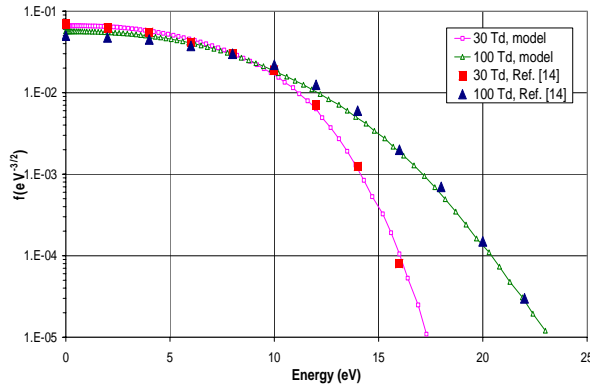


FIG. 1. Comparison of computed and calculated EEDF values for argon.

By applying Eq. (3), we calculated the average electron temperature (average electron energy) at various values of  $E/N$  and present these results in Fig. 2. We observe that  $T_e$  increases logarithmically for both pure argon and for the Ar/H<sub>2</sub> mixture as test gases.

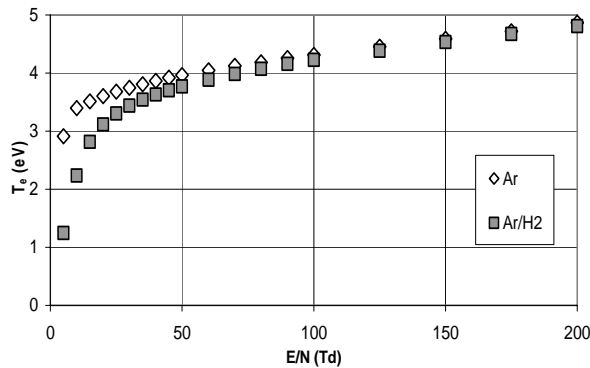


FIG. 2. Calculated values for the average electron temperature.

Additionally, the rate constants for transitions to the four 4s states of argon were calculated from Eq. (4), as shown in Fig. 3. Rate constants for transitions to the 4p and 3d states of argon were also calculated.

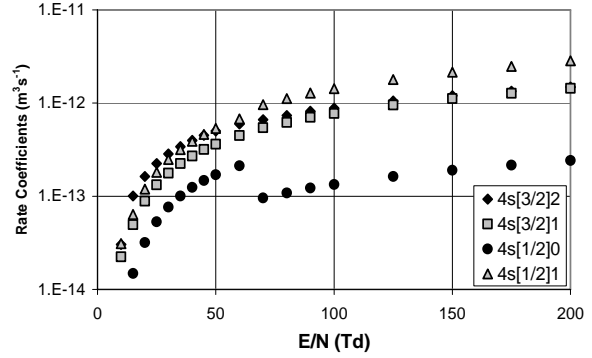


FIG. 3. Calculation of rate coefficients for the four 4s states of argon.

The last calculation which must be done to complete the kinetic model for our discharge is to calculate the value of the reduced electric field ( $E/N$ ). This will be done by coupling Eq. (2) with Poisson's equation,

$$\begin{aligned} \nabla^2 \Phi &= -\frac{\rho}{\varepsilon_0} \\ \frac{1}{s} \frac{\partial}{\partial s} \left( s \frac{\partial \Phi}{\partial s} \right) &= -\nabla \cdot \mathbf{E}. \end{aligned} \quad (5)$$

Then by applying the appropriate boundary conditions we will be able to perform the calculation.

In addition to the kinetic model, a chemical model must be formed for our discharge, in which the gas phase kinetics will be determined along with the significant reaction processes. Currently, the chemical model has not been completed.

### Experimental Approach

The experimental set-up for this study is a combination of supersonic flow tube and a

microwave cavity discharge. We used a commercial microwave generator to sustain a cylindrical cavity discharge at power density between 3.5 and 7 W/cm<sup>3</sup>, Fig. 4. The discharge extends along the length of the cavity as a surface discharge with gas temperatures between 900 and 1200 K. Using an evacuated quartz tube as a wave guide, supersonic discharge was generated with a cylindrical convergent-divergent (de Laval) nozzle downstream of the cavity. We estimate that the maximum electron density is about 10<sup>13</sup> cm<sup>-3</sup>.

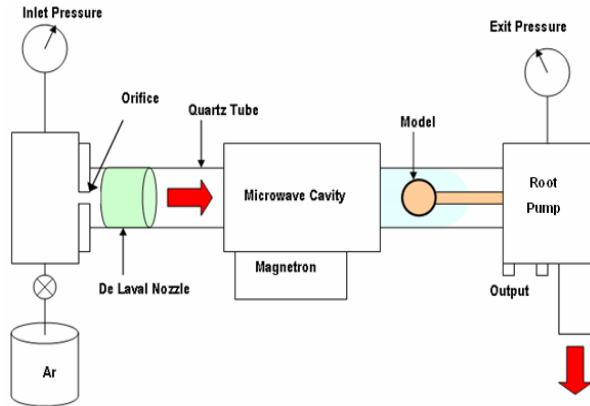


FIG. 4. Scheme of the supersonic flowing afterglow.

By varying the cross sectional area of the throat and exit of the nozzle we are able to increase or decrease the velocity of the flow. In Ar-H<sub>2</sub> (95/5%) gas with less than 0.01% N<sub>2</sub>, without any obstructions in the tube, we found experimentally that flow was generated up to M = 2.5 (Mach<sup>ii</sup>), as calculated by,<sup>15</sup>

$$M = \sqrt{2 \frac{\left(\frac{P_1}{P_2}\right)^{\frac{\gamma-1}{\gamma}} - 1}{\gamma-1}}. \quad (6)$$

<sup>ii</sup> A Mach number is defined as a number representing the ratio of the speed of a body to the speed of sound in a surrounding medium.

Here  $p_1$  is the ambient (or inlet) gas pressure,  $p_2$  is the exit gas pressure, and  $\gamma$  is the specific heat ratio.<sup>iii</sup>

Spherical models, made of Teflon, of diameter 10 mm and 16 mm were placed in the discharge and afterglow regions. For each model we are able to approximate the standoff distance for the shock wave.

To determine the standoff distance, we must assume that the flow directly in front of each of the spherical models along the axis of symmetry has a constant density, see Fig. 5 in which I have symbolized  $R_{shock}$  by a green line and  $R_{body}$  by a red line.

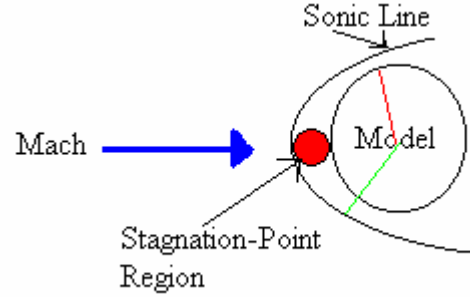


FIG. 5. Stagnation-point region for flow past a spherical model.

In the stagnation-point region,<sup>16</sup> the body to shock ratio,  $Y = \frac{R_{body}}{R_{shock}}$ , and the shock density ratio

$$\varepsilon = \frac{(\gamma-1)M^2 + 2}{(\gamma+1)M^2} \quad (7)$$

satisfies

$$3(1-\varepsilon)^2 Y^5 - 5(1-4\varepsilon)Y^3 + 2(1-\varepsilon)(1-6\varepsilon) = 0 \quad (8)$$

<sup>iii</sup> For the Ar/H<sub>2</sub> (95/5%) mixture  $\gamma = 1.65$  and for the pure argon = 1.67.

such that the relationship between the Mach number (M) and the standoff distance  $\delta = R_{\text{shock}} - R_{\text{body}}$  can be found from

$$\begin{aligned} \varepsilon &= \frac{b + \sqrt{b^2 - ac}}{a} \\ a &= 3(Y^5 + 4) \\ b &= 3Y^5 - 10Y^3 + 7 \\ c &= 3Y^5 - 5Y^3 + 2. \end{aligned} \quad (9)$$

Using the fact that  $R_{\text{body}}$  is approximately 5 mm for the small model, 8 mm for the large model, and  $\gamma$  for my mixture is 1.65, we are able to calculate the standoff distance for different Mach numbers. By comparing these results we see that the standoff distance decreases with increasing Mach number, see Fig. 6.

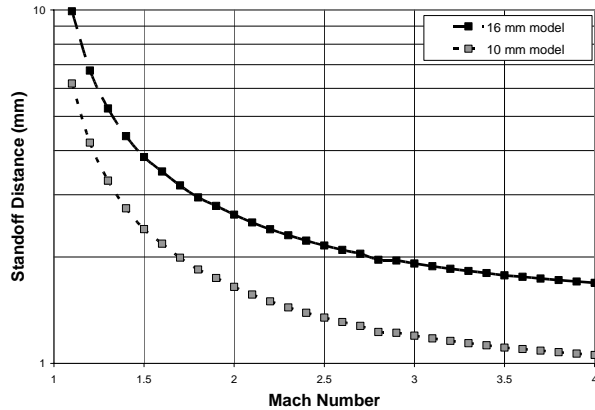


FIG. 6. Dependence of standoff distance on Mach number for argon.

### Data Collection and Analysis

From previous work done in our laboratory, it has been observed that the electronically excited states tend to accumulate at the location of a shock inside a supersonic flow.<sup>3-7</sup> By looking at the intensity of the radiation at different distances from the model, we are able to use the population at these distances as an indicator of a shock. The axial distribution of populations of excited states and the

enhancement of optical emission is observed by using a spectrometer in conjunction with a CCD camera, see scheme in Fig. 7.

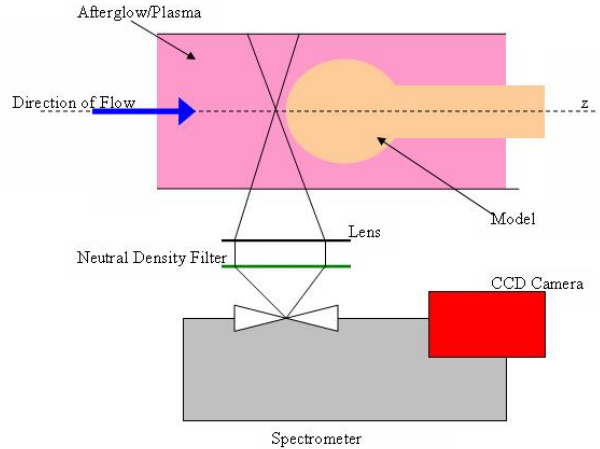


FIG. 7. Scheme of emission spectroscopy set-up.

Wavelengths were calibrated using a Spectra Physics Pen lamp and the intensity was calibrated using a Spectra Physics absolute blackbody irradiance source.<sup>6</sup> Graphs of irradiance per count versus wavelength were calculated for each grating. We can determine the populations of particular excited state transitions by using these irradiance per count versus wavelength graphs. We looked at three spectral lines during this part of our research, which have been identified in Fig. 8.

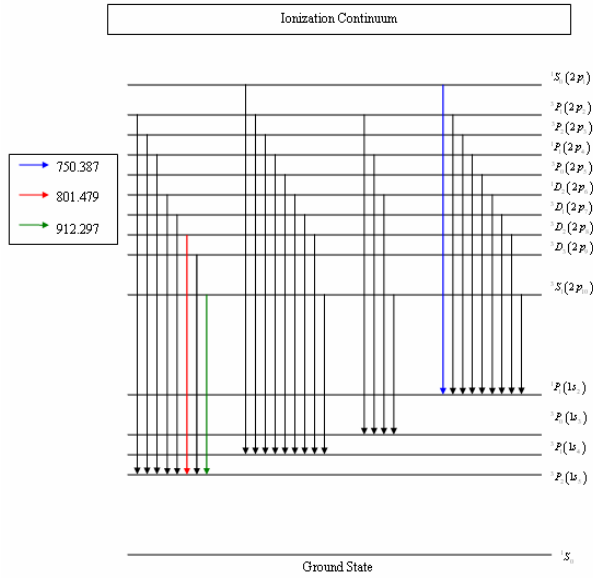


FIG. 8. Diagram of argon transitions<sup>17</sup>.

By taking the intensity of these spectral lines and multiplying by the irradiance per count for that wavelength, we can find the irradiance of that particular spectral line in  $\text{mW}/\text{m}^2(\text{nm})$ . Converting to  $\text{W}$  and  $\text{cm}^2$  and dividing by the length of the plasma region (about 2 cm), we find the irradiance ( $P_\lambda$ ) in terms of radiometric quantities ( $\text{W}/\text{cm}^3(\text{nm})$ ). Next, we converted from radiometric to photonic quantities by using

$$\frac{dN_p}{dt} = P_\lambda \cdot \lambda \cdot 5.03 \times 10^{15} \left( \frac{\text{ph}}{\text{cm}^3 \cdot \text{sec}} \right). \quad (10)$$

Finally, we were able to calculate the population ( $N_u$ ) by using Eq. (11).<sup>18</sup>

$$N_u = \frac{dN_p}{dt} \left( \frac{1}{A_{ul} \cdot g_u} \right) \quad (11)$$

We first looked at the populations of excited states in a model free afterglow as shown in Fig. 9. By comparing the population values with a Boltzmann plot (straight line), we can see that as we went to higher energy levels,

the population decreased. This effect was more pronounced at the higher power density.

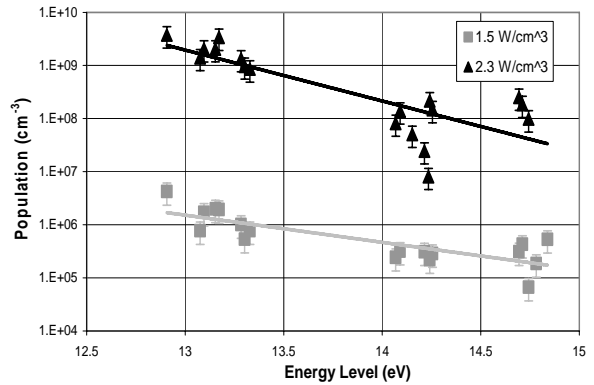


FIG. 9. Population of argon excited states in a model free afterglow.

Next, we looked at the gas kinetic temperature along a model free flow. By inserting a thermal couple into the gas, we were able to measure the temperature along the flow at various power densities. We can see from Fig. 10 that as we move away from the edge of the microwave cavity (0 mm position) the temperature along the flow decreases by approximately 150 K.

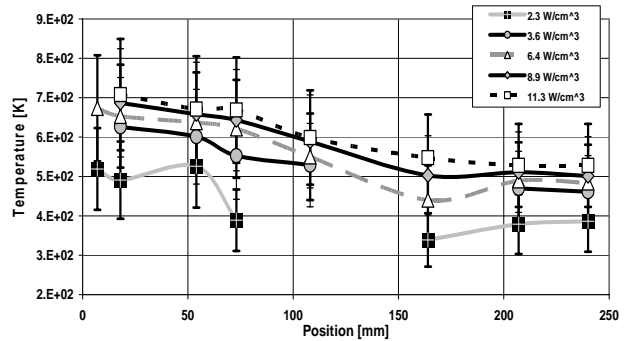
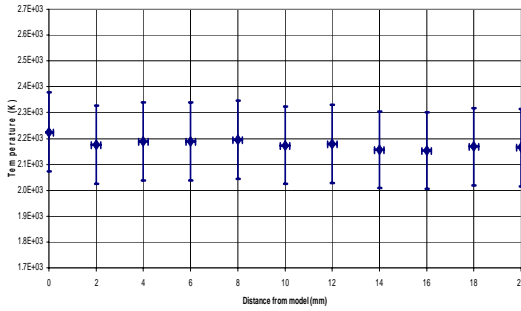
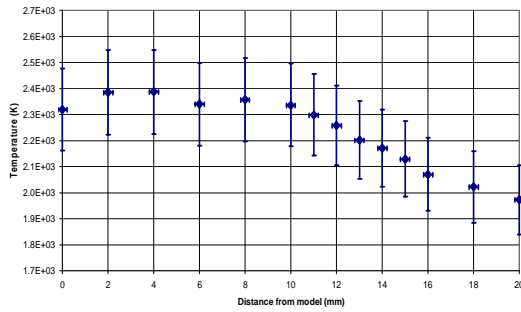


FIG. 10. Gas kinetic temperature along a model free argon afterglow.

Now that we had a rough idea of what the plasma is doing without the model, we inserted the 16 mm diameter model into the flow. We began by looking at the electron excitation temperature both in static and dynamic conditions, see Fig. 11 a, b.



(a)



(b)

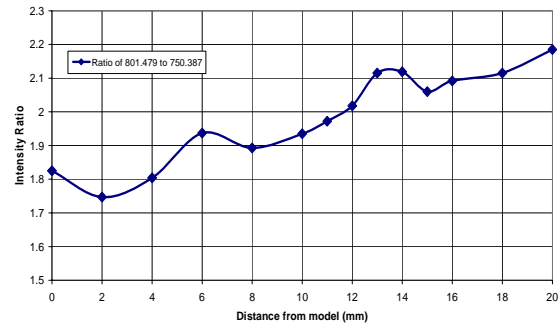
FIG. 11. Electron excitation temperature of argon 4p levels under static (a) and dynamic (b) conditions.<sup>iv</sup>

In Fig. 11a, we observe that in static conditions, the temperature remains relatively constant at about 2200 K. On the other hand, in Fig. 11b we observe that the temperature varies greatly with distance along the axis of the flow. From these diagrams, it is clear that the shock waves, which form in front of the model, do have an impact on the temperature of the flow.

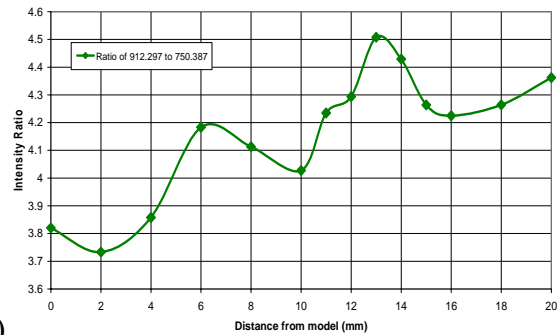
Additionally, we looked at the ratio of intensities of 4p transitions, shown in Fig. 12 a, b. From these graphs we observe that there are distinct peaks at 6 mm and 13 mm in the ratios. This data leads us to conclude that we do have a strong shock wave which is being dispersed along the axis of flow. Taking the standoff distance to be 6 mm for our 16 mm diameter model, we can estimate the Mach

<sup>iv</sup> Error bars in the y-direction are due to scattering by the quartz tube. Error bars in the x-direction are associated with the precision to which we can measure the position of the model.

number, from Fig. 6, of the shock front to be 1.5.



(a)



(b)

FIG. 12. Ratio of intensities of the highest 4p level to the lowest 4p transitions for argon.

### Concluding Remarks

The primary objective of our research is to understand the double electric layer formed by the mutual interaction of an acoustic shock wave and a weakly ionized discharge and to determine the strength of this double layer. We found that there was evidence of optical emission enhancement at the shock front, which is an indicator of a double electric layer. Additionally, we observed the dispersion of the shock wave along the axis of flow. From these dispersion patterns, we estimated that the experimental standoff distance for the shock wave to be 6 mm for the 16 mm diameter model with an associated mach number of 1.5.

To validate the hypothesis of a strong double electric layer, we will need to determine the

mean electron temperature differences between the plasmas, since the strength of this difference determines the strength of the double layer.<sup>19</sup> Additionally, we plan to upgrade our nozzle to sustain a model free flow up to  $M = 7$ .

Using the data from experiment and current understanding of ionization and excitation processes in microwave discharge plasmas, we plan to explore the effects of local increase of excited and ionized states on excessive local heating. Furthermore, we plan to explore the role of radiation trapping on the dynamic and structural properties of the shock wave modified by the plasma.

We also plan to extend our research to Martian atmospheric entry conditions. We will employ a Martian Simulated Gas<sup>v</sup>, which will allow us to simulate the composition of the atmosphere. We will evaluate the EEDF for the primary gas molecules during discharge: CO<sub>2</sub>, CO, O<sub>2</sub>, O, N<sub>2</sub>, and Ar. The associated transport parameters will be calculated.

In addition, we will calculate the jump conditions using NASA's Viking, Pathfinder, and MER Opportunity probe data. From these results, the electron density will be determined for each probe from Saha's equation. This will enable us to calculate the species concentrations given in the chemical model developed in Ref. [20]. Since many of the arguments<sup>3-10</sup> refer to molecular properties of plasma constituents, we will be in a position to compare the results in pure monatomic and in molecular gases.

Data from this experiment has been presented at the 59<sup>th</sup> Annual Gaseous Electronics Conference<sup>4</sup> and the 73<sup>rd</sup> Annual Meeting of

the Southeastern Section of the American Physical Society.<sup>5</sup> This research was also presented at the 2007 Spring Research Symposium for the College of Sciences at Old Dominion University.

- 
- [1] Y. Z. Ionikh, N. V. Chernysheva, A. V. Meshchanov, A. P. Yalin, and R. B. Miles, *Phys. Lett. A* **259** (1999) 387.
  - [2] A. F. Aleksandrov, N. G. Vidyakin, V. A. Lakutin, M. G. Skvortsov, I. B. Timofeev, and V. A. Chernikov, *Sov. Phys. Tech. Phys.* **31** (1986) 468.
  - [3] S. O. Macheret, Y. Z. Ionikh, N. V. Chernysheva, A. P. Yalin, L. Martinelli, R. B. Miles, *Phys. Fluids* **13** (2001) 2693.
  - [4] D. J. Drake, J. Uphaday, S. Popovic, L. Vuskovic, *Double Electric Layer in Stationary Shock Structures of a Supersonic Flowing Afterglow*. 59<sup>th</sup> Annual Gaseous Electronics Conference, Columbus, Ohio, October 2006, p. 67 (SRP2 36).
  - [5] D. J. Drake, J. Uphaday, S. Popovic, L. Vuskovic, *Stationary Shock Wave Structures in a Microwave Flowing Afterglow*. 73<sup>rd</sup> Annual Meeting of the Southeastern Section of the APS, Williamsburg, VA, November 2006, p. 32 (GC.00014).
  - [6] S. Popović, L. Vuskovic, *Phys. Plasmas* **6** (1999) 1448.
  - [7] L. Vušković, S. Popović, J. Drake, R. W. Moses, *Magnetohydrodynamic Power Generation in the Laboratory Simulated Martian Entry Plasma*, Proc. XV International Conference on MHD Science and Applications, ed. V. Bityrin, pp 150-55, IVTAN, Moscow, May 2005.
  - [8] P. Bletzinger, B. N. Ganguly, A. Garscadden, *Phys. Plasmas* **7** (2000) 4341.
  - [9] P. Bletzinger, B. N. Ganguly, D. Van Wie, A. Garscadden, *J. Phys., D: App. Phys.* **38** (2005) R33.
  - [10] N. Siefert, B. N. Ganguly, P. Bletzinger, *Phys. Rev. E* **72** (2005) 066402(6).

---

<sup>v</sup> Martian Simulated Gas (MSG) consists of 95.7% CO<sub>2</sub> with minor concentrations of N<sub>2</sub> (2.75%) and Ar (1.55%).

- [11] P. Kessaratikoon, S. Popović, L. Vušković,  
*Dispersion and Propagation of Weak Shock  
Waves through Microwave Cavity Discharges*,  
AIAA 2004-1021 (American Institute of  
Aeronautics and Astronautics).
- [12] L. S. Frost, A. V. Phelps, Phys. Rev. **127** (1962)  
1621.
- [13] J. Lowke, A. V. Phelps, B. W. Irwin, J. Appl. Phys, **44**  
(1973) 4664.
- [14] C. M. Ferreria, J. Loureiro, J. Phys D: Appl. Phys,  
16 (1983) 2471.
- [15] J. D. Anderson, *Modern Compressible Flow*,  
McGraw Hill, Boston, 2003.
- [16] M. Rasmussen, *Hypersonic Flow*, Wiley, New  
York, 1994.
- [17] D. B Atkinson, M. A. Smith, Rev. Sci. Instr. **66**  
(1995) 4434.
- [18] R. S. Stewart, D. J. Smith, J. Phys D: Appl. Phys.  
**35** (2002) 1777.
- [19] P. Bletzinger, B. N. Ganguly, A. Garscadden,  
Phys. Rev. E **67** (2003) 047401(4).
- [20] T. Dinh, *Decomposition of Carbon Dioxide in a  
Capacitively coupled Radio Frequency Discharge*,  
Doctoral Dissertation, (Old Dominion University  
2002).